Journal of Solid State Chemistry 181 (2008) 1614–1620

Contents lists available at ScienceDirect

Journal of Solid State Chemistry

journal homepage: www.elsevier.com/locate/jssc

Synthesis and catalytic properties of microemulsion-derived cerium oxide nanoparticles ☆

Emanuel Kockrick [a], Christian Schrage [a], Anett Grigas [a], Dorin Geiger [b], Stefan Kaskel [a,*]

[a] Department of Inorganic Chemistry, Dresden University of Technology, Mommsenstr. 6, D-01062 Dresden, Germany
[b] Triebenberg Laboratory for HRTEM and Electron Holography, Institute for Structure Physics, Dresden University of Technology, Zum Triebenberg 50, D-01328 Dresden, Germany

ARTICLE INFO

Article history:
Received 31 January 2008
Received in revised form
11 April 2008
Accepted 23 April 2008
Available online 8 May 2008

Keywords:
Ceria nanoparticles
Inverse microemulsion
Small angle X-ray scattering
Dynamic light scattering
Catalysis
Soot combustion

ABSTRACT

The synthesis of cerium dioxide nanoparticles using an inverse microemulsion technique and precipitation method was investigated. Cerium hydroxide nanoparticles were synthesized by adding diluted ammonia to *n*-heptane–surfactant–cerium nitrate system. The micelle and particle size in the range of 5–12 nm were controlled by varying the molar water to surfactant ratio and analyzed by dynamic light scattering (DLS), small angle X-ray scattering (SAXS) and high-resolution transmission electron microscopy (HRTEM). Cerium hydroxide nanoparticles were isolated and subsequently treated at 100–600 °C to obtain nanoscale ceria. Crystallite sizes of cerium dioxide in the range of 6–16 nm were estimated by Scherrer analysis by X-ray diffraction (XRD) and HRTEM. The catalytic activity of particles annealed at 400 and 600 °C in soot combustion reactions was characterized by temperature-programmed oxidation (TPO) indicating a size-dependant activity. Crystallite sizes and catalytic stability of elevated ceria systems were tested in second combustion cycles.

1. Introduction

Nanostructured inorganic particles are promising systems as oxidation catalysts due to the high surface to volume ratio. Especially, nanoscale cerium dioxide containing systems are a very attractive three-way catalyst systems for soot combustion reactions and were reported by several groups [1,2]. The reason for the catalytic effect is oxygen donation of CeO_2 caused by partial Ce^{4+}/Ce^{3+} reduction on the surface of catalyst particles [3]. This effect can be further increased, using CeO_2–ZrO_2 solid solutions and compounds or doping with transition and rare-earth metals [4–7]. Ceria can be used as a water–gas shift catalyst in combination with precious transition metals [8,9]. Several methods were developed for the preparation of CeO_2 nanoparticles, such as chemical vapor deposition routes [10], flame spray pyrolysis [11], precipitation synthesis [6,12] and template-assisted techniques in ordered mesoporous silica [13,14]. Also various microemulsion techniques were developed for the synthesis of nanoscale ceria systems [4,15–18]. However, for the preparation of highly active nanoscale catalysts a high dispersion and accessibility of active centers on a support is necessary.

In the following, we describe the synthesis of cerium dioxide nanoparticles using the inverse microemulsion technique and we investigate the catalytic activity of CeO_2 nanoparticles in the soot combustion reaction. A microemulsion is a ternary thermodynamic stable system consisting of a non-polar oil phase, a surfactant (and co-surfactants), and a polar phase. In inverse microemulsion systems, nanoscale aqueous phases are dispersed in a continuous oil phase [19,20]. The micelle and particle size can be precisely defined by the molar water to surfactant ratio (R_W value). Several nanostructures could be prepared by this method such as elements [21,22], or different chalcogenide structures [20,23–25], and complex oxide compounds [26–28]. Precipitation processes of alkoxides and nitrates in the polar phase form nanoscale structures determined by the micelle size [18,29]. The particles can be isolated, destabilizing the microemulsion and redispersed in another medium [30]. The microemulsion method is also suitable for the direct preparation of inorganic nanoparticles inside a polymer or ceramic structures [31–33].

The resulting nanocomposites combine the properties of inorganic guest structure with the characteristics of the host material. Therefore, catalytic active species like ceria can be synthesized and incorporated in preceramic materials like polycarbosilanes. Thus, the resulting composite combines the catalytic activity of the incorporated ceria nanoparticles and the hardness of the support material.

Scheme 1 shows the principle of the synthesis strategy of cerium dioxide nanoparticles using the inverse microemulsion

☆ Financial support by the German Research Foundation (KA 1698/6-1) in the NanoMat Program SPP 1181 is gratefully acknowledged.
* Corresponding author. Fax: +49 351 46337287.
E-mail address: stefan.kaskel@chemie.tu-dresden.de (S. Kaskel).

0022-4596/$ - see front matter © 2008 Elsevier Inc. All rights reserved.
doi:10.1016/j.jssc.2008.04.036

technique, which is similar to our recently published studies [33]. Different ratios of an aqueous cerium nitrate solution and a non-ionic surfactant are dissolved inside *n*-heptane, as continuous oil phase to form nanoscale water droplets inside the oil matrix. Subsequently, diluted ammonia is added to precipitate the cerium hydroxide inside the nanoreactor (Scheme 1, Step 1). For isolation of the ceria nanoparticles, an acetone/ethanol mixture is added to destabilize the yellow colored, transparent dispersion followed by filtration and drying processes of the precipitate (Scheme 1, Steps 2 and 3). Afterwards the ceria nanoparticles are annealed at 400–600 °C to promote crystallization and remove organic residues (Scheme 1, Step 4). The catalytic activity of pre-annealed ceria nanoparticles is tested in soot combustion reaction using the temperature-programmed oxidation (TPO, Scheme 1, Step 5).

The particle size of the resulting cerium dioxide could be controlled by the molar water to surfactant ratio (R_W value) and the thermal treatment in the range of 6–16 nm. Catalytic investigations show a size-dependant activity in soot combustion reactions.

2. Experimental

2.1. Synthesis of cerium oxide nanoparticles

All chemicals were used as received. 26.9 g of an aqueous 0.2 M $Ce(NO_3)_3$ solution ($Ce(NO_3)_3 \cdot 6H_2O$, Aldrich, 99%), 273.6 g *n*-heptane (Sigma-Aldrich, >99%) and a defined mass of the non-ionic surfactant Marlophen NP 5 ($RO(CH_2CH_2O)_xH$, $x = 5$, R = nonylphenyl, $M = 440\,g\,mol^{-1}$, SASOL) were mixed according to R_W values (molar water to surfactant ratio) at 28 °C as listed in Table 1.

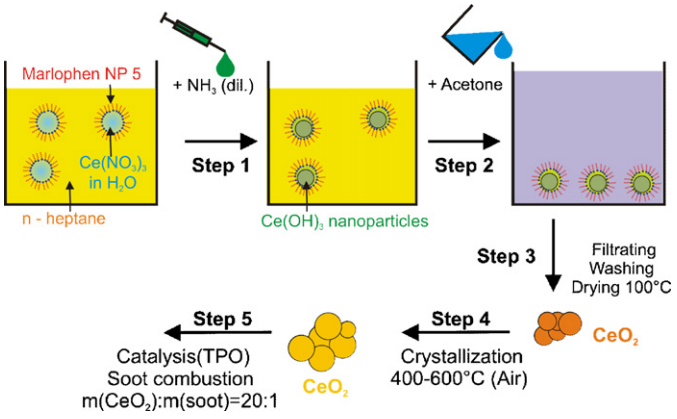

Scheme 1. Schematic synthesis strategy for preparation of ceria nanoparticles: Starting system consisting of inverse microemulsion with aqueous cerium precursor, Step (1) precipitation of nanoscale $Ce(OH)_3$ particles inside micelle structure by adding diluted ammonia, Step (2) addition of acetone to transparent dispersion to destabilize the microemulsion system, Step (3) filtration, washing and drying steps to isolate cerium dioxide nanoparticles, Step (4) oxidative treatment of CeO_2 nanoparticles to promote crystallization and remove organic residues, and Step (5) testing catalytic activity of different ceria systems in soot combustion.

The viscosity of all transparent microemulsions was measured after 1 h at 28 °C with a Ubbelohde viscosimeter Type 532-13Ic by Schott. The mean value out of five measurements is given. The inverse microemulsion systems containing the cerium salt were stirred for 1 h in a closed 1 l flask at 28 °C. Then, 2.04 g of diluted ammonia solution (Sigma-Aldrich, 2.5 wt%) were added drop-wise to the transparent microemulsion system and stirred for another hour at 28 °C. For the isolation of cerium hydroxide particles, an excess of acetone was added to the particle dispersion and stirred for 48 h at room temperature followed by filtration and several washing processes. The brown residue was dried at 100 °C over night followed by subsequent treatment at 400 and 600 °C for 1 h with a heating ramp of 5 °C/min.

2.2. Catalytic oxidation of commercially available soot

Catalytic activity of ceria nanoparticles was investigated in a TPO for the determination of the peak combustion temperature (T_{Max}). The 100 mg of ceria samples annealed at 400 and 600 °C were mixed in a mortar for 15 min with 5 mg of commercial available soot (Printex V, Evonik AG) in defined ratios of 20–1. The mixtures were transferred to a U-type quartz reactor and heated up with a constant temperature ramp of 10 °C/min under defined gas mixture 10 scm^3 (94 vol% helium, 6 vol% oxygen) up to 700 °C.

2.3. Characterization

The inverse microemulsion systems were characterized by dynamic light scattering (DLS) using a Zetasizer Nano ZS from Malvern Instruments. The micelle sizes in the microemulsion as well as the hydroxide particle size after ammonia addition were measured at 28 °C. For DLS experiments, the measured viscosities of inverse microemulsions were used. The average particle diameters (*z*-average) and polydispersity indices (PDI) were determined using a cumulant analysis. PDI values are parameters, expressing the degree of monodispersity in the system (values below 0.1 characterize the system as monomodal distributed). Intensity weighed size distributions were calculated using a non-negative least-square algorithm (NNLS) [34].

The small angle X-ray scattering (SAXS) experiments were carried out in transmission mode on a Bruker Nanostar with Cu$K\alpha_1$ radiation ($\lambda = 0.15405$ nm) and a position sensitive HiStar detector. The samples were prepared in a sealed quartz capillary with a diameter of 2 mm at 28 °C. Samples for TEM analysis were prepared by dipping carbon-coated copper grids into microemulsions after precipitation of cerium hydroxide or into an ethanol suspension of ceria particles. TEM investigations were performed on the Cs-corrected 200 kV-TEM FEI Tecnai F20 Cs-corr at the Triebenberg-Laboratory for high-resolution TEM and electron holography. The spherical aberration correction (Cs-correction) allows a precise estimation of lateral dimensions avoiding errors due to delocalization effects. These are caused by a high spherical aberration in conventional TEM. X-ray powder diffraction patterns were recorded in transmission geometry using a Stoe Stadi-P diffractometer with image plate detector and Cu$K\alpha_1$ radiation. Size broadening of peaks in the range from $2\Theta = 20$–80° was analyzed

Table 1
Sample codes, composition and viscosities of the microemulsion systems used

Sample name	R_W	$m_{n\text{-Heptane}}$ (g)	$m_{Ce(NO3)3,aq}$ (g)	$m_{Marlophen}$ (g)	Viscosity (mm^2/s)	$m_{NH3,dil}$ (g)
Ce-5.8	5.8	273.6	26.9	98.7	2.75	2.04
Ce-11.7	11.7			49.3	1.97	
Ce-16.4	16.4			36.0	0.97	

using the Stoe size/strain analysis based on Debye–Scherrer equation [35]. Instrumental broadening was taken into account based on LaB_6 reference measurements. TPO was investigated using a Quantachrome ChemBet 3000 with thermal conductivity detector. The catalyst soot mixture was prepared by intensive mixing of ceria nanoparticles and a standard soot (Printex V, Evonik AG) in a defined mass ratio of 20:1 using a mortar for 10 min. 100 mg of the mixture was heated up in a defined 94 vol% Helium (Air Liquide 4.6)/6 vol% oxygen ratio (Air Liquide 5.0) with a total flow rate of 10 sccm/min and a temperature ramp of 5 °C/min up to 700 °C. The reactor temperature was analyzed by a Ni/Cr/Ni thermocouple located in the catalyst bed. In order to test reproducibility, a series of three tests was carried out. Within a range of 10 °C T_{MAX} was reproducible.

3. Results and discussion

3.1. Inverse microemulsions and cerium hydroxide nanoparticles

The DLS experiments revealed increasing hydrodynamic diameters for micelles as well as for precipitated particles with increasing R_W value, shown in Fig. 1. Referring to this technique the sizes were adjustable from 2.5 to 9.5 nm by changing the R_W from 5.8 to 16.4 (Table 2). Because the PDI values were below 0.1 in all cases, one can say that nearly no particle growth and no aggregation occurred during the ceria formation within the micelles.

Additionally SAXS was used to characterize micelles and particles. The shift of the background corrected scattering curves to lower q values with higher R_W values shown in Fig. 2 proofs an increasing particle size. To evaluate SAXS data one can use the GUNIER approximation [36] (Eq. (1)). This approximation is valid for the inner part of scattering function ($0 < q < 1{,}3R_G$) and reveals the radius of gyration R_G

$$I(q) = \overline{q^2}V^2\, e^{-q^2R_G^2/3} \quad (1)$$

Eq. (1) Guinier's Law; q scattering vector; V scattering volume; R_G radius of gyration.

When assuming spherical particles the radius of the micelle or particle r_{Sphere} is obtained as follows:

$$r_{Sphere} = R_G/\sqrt{\frac{3}{5}} \quad (2)$$

However, the particle shape has to be known to get the right radii. To get more detailed information about the particle shape, methods using inverse Fourier transformations [37] or full profile fitting programs [38] are very useful. These methods give additional size information.

An inverse Fourier transformation (Eq. (3)) of a scattering function leads to so-called pair distance distribution function (PDDF) $P(r)$

$$P(r) = [1/(2\pi^2)] \int_0^\infty I(q)(qr)\sin(qr)\,dr \quad (3)$$

The PDDF for spherical particles has to be symmetric, while rods or ellipsoids give asymmetric PDDFs [36]. These calculations were carried out with the program GNOM [37] revealing PDDFs which are typical for spherical particles (see Supporting Information S1).

Another useful evaluation is the full profile fitting of the scattering functions. Here, theoretical scattering functions of different particle shapes can be fitted to the experimental curves by least-square algorithms. In this way, information about shape and size of the scattering bodies as well as a size distribution is obtained. These evaluations with the program NanoFit [38]

Table 2
Micelle diameter and particle size of cerium nitrate containing inverse microemulsion before and after ammonia addition estimated by dynamic light scattering (DLS) and small angle X-ray scattering (SAXS)

Method	Sample code[a]					
	Ce-5.8		Ce-11.7		Ce-16.4	
	ME	Particles	ME	Particles	ME	Particles
DLS d_{DLS} (nm) (PDI)	2.5 (0.05)	2.1 (0.06)	4.6 (0.10)	6.1 (0.08)	8.9 (0.04)	9.4 (0.06)
SAXS d_{SAXS} (nm)						
GUINIER	5.1	5.1	7.5	7.5	9.4	9.6
GNOM	5.9	5.8	9.3	9.4	11.6	12.4
NANOFIT	5.6±1.2	5.8±1.2	8.6±1.8	8.4±1.9	11.1±2.3	11.9±2.5

[a] Sample code Ce-XX-YYY-Z: XX: R_W value as molar water to surfactant ratio, YYY: pre-annealing temperature of ceria nanoparticles at 400 and 600 °C, Z Sample abbreviation after first and second temperature-programmed oxidation (I/II). GUINIER, GNOM, and NANOFIT refer to the different calculation methods compared (see text).

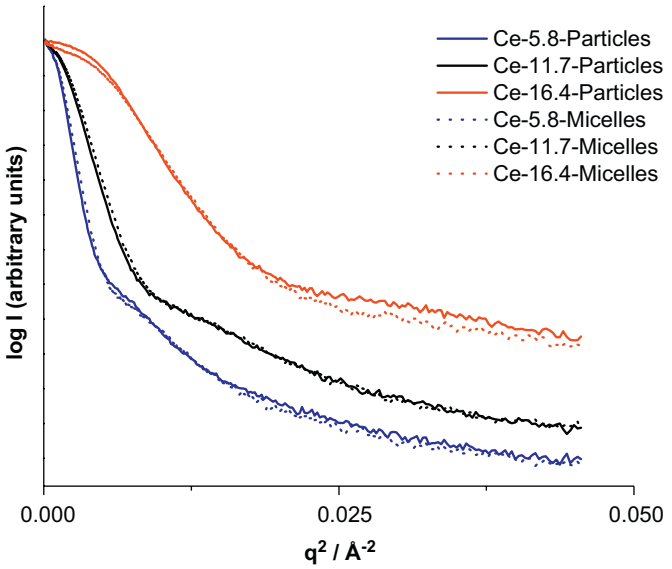

Fig. 2. Small angle X-ray scattering curves of inverse microemulsions and particle dispersions.

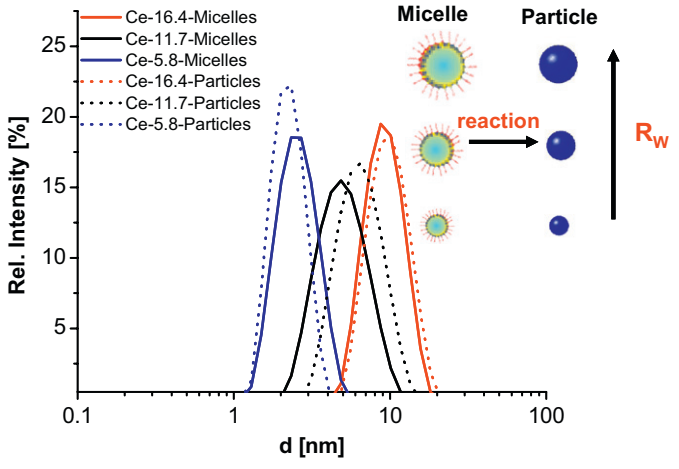

Fig. 1. DLS curves of inverse microemulsions and particle dispersions.

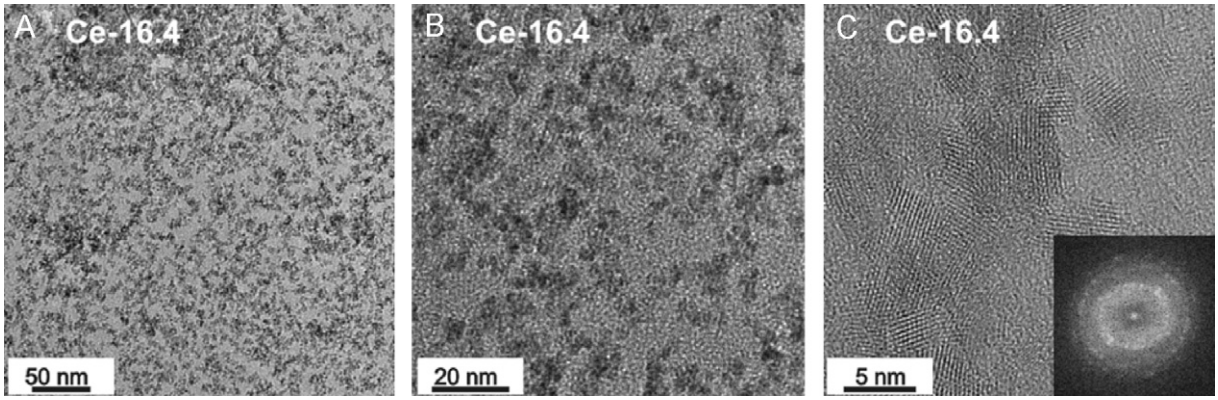

Fig. 3. TEM images of $Ce(OH)_3$ nanoparticles with R_W of 16.4 after ammonia addition.

confirmed the spherical shape of micelles as well as ceria particles.

The results of the SAXS and DLS experiments show a decreasing particle size with decreasing R_W values (Table 2). However, a slight mismatch is observed at lower R_W values which will be discussed in the following. The high surfactant ratio within the inverse microemulsions with a R_W value of 5.8 and 11.7 leads to a very high concentration of micelles. Because the Stokes–Einstein equation in the DLS evaluation is only valid for very dilute systems, the resulting hydrodynamic diameters are underestimated [39]. Thus, the application of DLS is limited to dispersions of low concentrations of micelles and SAXS can be a useful technique to characterize dispersions with higher surfactant ratio. The latter explains the discrepancy between d_{DLS} and d_{SAXS} for the sample with an R_W value of 5.8 and 11.7.

Transmission electron microscopy was used to characterize the microemulsion system with $R_W = 16.4$ after ammonia addition (Scheme 1, Step 1). Fig. 3 shows regular particles in the range of 2–3 nm with spherical shape. Lattice fringes can be observed in high-resolution TEM images (Fig. 3C). The *d*-spacings in Fig. 3C were determined from the reflections in the electron diffractogram (Fourier-transformation) of the TEM images. Lattice spacings of 3.23, 2.78 and 1.99 Å, corresponding to the (110), (200) and (002) reflections of cerium hydroxide (3.250, 2.820 and 1.914 Å) were observed [40].

3.2. Cerium oxide nanoparticles

The precipitated cerium hydroxide nanoparticles with different R_W values were dried at 100 °C (Ce-R_W-100; Scheme 1, Step 3) followed by subsequent annealing at 400 and 600 °C (Ce-R_W-400/600, Scheme 1, Step 4) to promote the crystallization of cerium dioxide and remove organic residues (surfactant). For additional studies, ceria particles were prepared using a simple precipitation of cerium nitrate with concentrated ammonia (Ce-Prec). Diffraction patterns of Ce-16.4 annealed at different temperatures are presented in Fig. 4 showing broad peaks already after drying at 100 °C. The nanocrystalline ceria phase corresponds to cerium dioxide [41]. The crystallite size for all microemulsion-based ceria systems (Ce-R_W) and precipitated nanoparticles (Ce-Prec) increases using higher oxidation temperature as presented in Table 3. However, after drying at 100 °C and annealing at 400 °C, the particle sizes remain almost constant for all R_W values (Ce-16.4-100: 9.4 nm; Ce-16.4-400: 9.6 nm). By increasing the annealing temperature up to 600 °C, the crystallite sizes strongly increases from 6.1 nm (Ce-5.8-600) up to 16.4 nm (Ce-5.8-600). This can be explained by sintering processes and particle

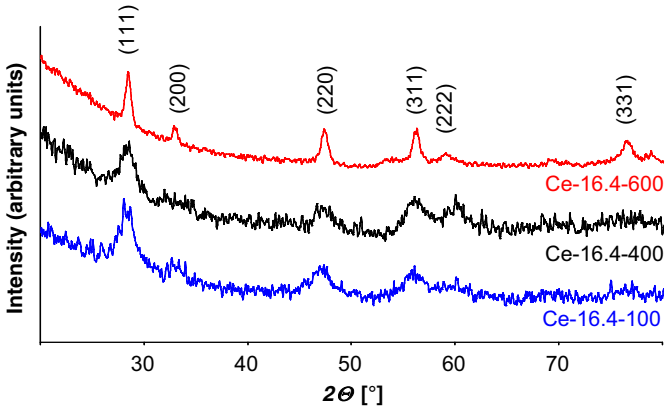

Fig. 4. X-ray diffraction patterns of ceria nanoparticles with R_W of 16.4 annealed at various different temperatures.

Table 3
Crystallite sizes of ceria nanoparticles synthesized by inverse microemulsion method for various R_W-values and precipitation technique oxidized at 100–600 °C

T (°C)	Crystallite size (nm)[a]							
	Ce-5.8		Ce-11.7		Ce-16.4		Ce-Prec	
	Fresh	After TPO	Fresh	After TPO	Fresh	After TPO	Fresh	After TPO
100	6.0	–	6.2	–	9.4	–	17.3	–
400	6.1	17.6	8.5	14.7	9.6	28.0	17.8	32.1
600	16.4	21.3	12.9	24.0	14.0	31.2	20.3	33.4

[a] Crystallite size estimated from peak broadening using Scherrer method.

agglomeration taking place at this temperature. Ceria nanoparticles prepared by the precipitation method contain significantly larger particle sizes (Ce-Prec-400: 17.8 nm) as compared to microemulsion-derived nanoparticles (Ce-16.4-400: 9.6 nm). However, the crystallite size of these ceria particles only smoothly increases by annealing at 600 °C (Ce-Prec-600: 20.3 nm). For inverse microemulsion-based systems the micelle and resulting particle size can be controlled by the R_W value (the molar water to surfactant ratio) and was already discussed above. According to Table 3, also the crystallite size for ceria systems annealed at 100 and 400 °C increases from 6.1 nm (Ce-5.8-400) to 8.5 nm (Ce-11.7-400) and up to 9.5 nm (Ce-16.4-400). The crystallite sizes of Ce-R_W-100 and Ce-R_W-400 show a good agreement to the

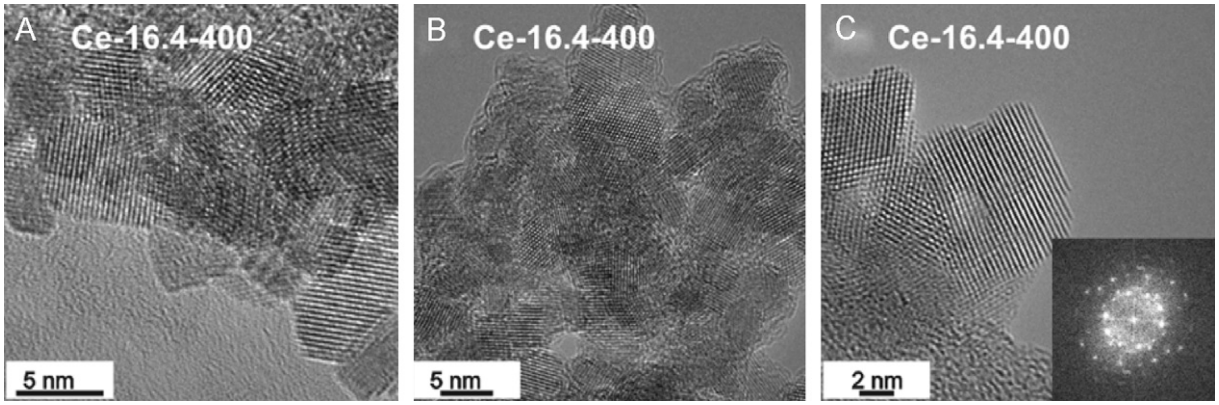

Fig. 5. High-resolution transmission electron micrographs of ceria nanoparticles ($R_W = 16.4$) oxidized at 400 °C (Ce-16.4-400)

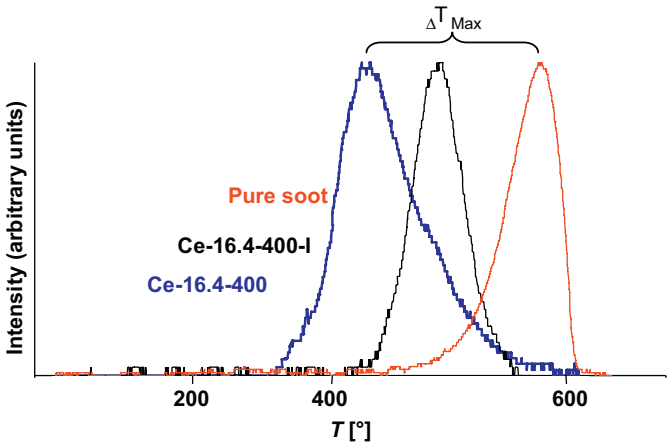

Fig. 6. Catalytic activity of Ce-16.4-400 nanoparticles in first and second catalytic cycle compared to non-catalyzed soot combustion (pure soot).

particle sizes estimated by SAXS and DLS investigations. (Table 2) Transmission electron micrographs presented in Fig. 5 of ceria particles annealed at 400 °C (Ce-16.4-400) show agglomerated nanostructures in the size range of 6–8 nm which corresponds to the crystallite size of 9.6 nm calculated using the Scherrer equation in X-ray diffraction (XRD) (Fig. 4 and Table 3). In high-resolution TEM the lattice distances could be estimated to be 3.14, 2.70, 1.91 and 1.58 Å, which corresponds to the (111), (200), (220) and (311) *d*-spacings of CaF_2-type cerium dioxide (3.125, 2.706, 1.914, 1.632 Å) [41].

3.3. Catalytic investigations

Catalytic soot combustion of ceria nanoparticles annealed at 400 and 600 °C was carried out using the TPO in a micro-flow reactor with a thermal conductivity detector (Scheme 1, Step 5). The catalytic activity for nanoparticle systems was defined by the maxima in the detector signal vs. temperature plots (Fig. 6). All ceria systems show catalytic activity, because the maximum is decreased up to 236 °C (Ce-11.7-400) compared to non-catalysed soot combustion and is presented in Table 4. Ceria systems annealed at 400 °C show a higher depression of the soot ignition temperature (Ce-5.8-400: 417 °C) than nanoparticles heat treated at 600 °C (Ce-5.8-600: 501 °C). These results show a good agreement to the smaller crystallite sizes for particles annealed at 400 °C (Ce-5.8-400: 6.1 nm; Ce-5.8-600: 16.4 nm), which were

Table 4
Catalytic activity of ceria nanoparticles with different R_W values annealed at 400 and 600 °C in soot combustion reactions

T_{ceria} (°C)	T_{MAX} (°C)[a]				
	Ce-5.8	Ce-11.7	Ce-16.4	Ce-Prec[b]	Pure soot
400	417	404	414	408	640
600	501	476	461	433	

[a] Estimated by signal maximum in TPO method.
[b] Reference prepared by precipitation.

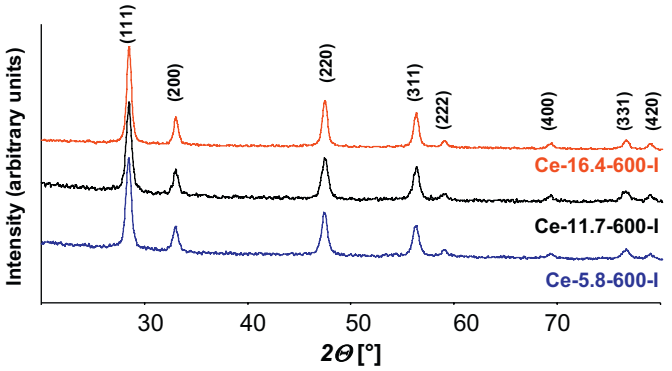

Fig. 7. X-ray diffraction patterns of ceria nanoparticles for different R_W after temperature-programmed oxidation (TPO).

already discussed above. However, for particles heat treated at a constant temperature, no size-dependant temperature maximum could be observed, and smaller particles in Ce-5.8-400 show almost the same temperature maximum (417 °C) than larger Ce-16.4-400 particles (414 °C). This effect can be explained by agglomerated particles shown in Fig. 5A and B, which limit the catalytically active surface. Microemulsion-derived ceria nanoparticles annealed at 400 °C have almost the same catalytic activity as precipitated CeO_2 particles (Ce-Prec-400: 408 °C). However, catalytic passivation of Ce-Prec-600 (433 °C) nanostructures is significantly lower than for ceria particles synthesized by the inverse microemulsion method, because the crystallite sizes remain almost constant (Table 3). After the TPO, solid catalyst residues were characterized using X-ray powder diffraction methods presented in Fig. 7. Only the cerium dioxide phase could be identified. Additionally, an increase in crystallite sizes by

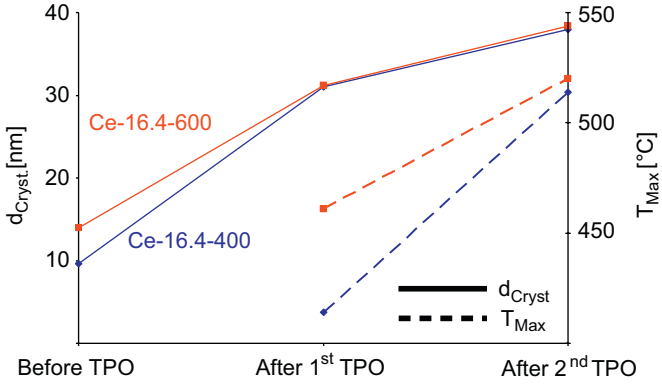

Fig. 8. Testing the catalytic stability (T_{Max}, TPO) of ceria nanoparticles ($R_W = 16.4$) annealed at 400° and 600 °C in two catalytic cycles and investigating the crystallite sizes (d_{Cryst}, XRD) before and after catalytic test.

smaller peak widths of all ceria particle systems results caused by sintering processes at testing temperatures in the TPO upto 700 °C as listed in Table 3. However, particles pre-annealed at 400 °C (Ce-11.7-400-I: 14.7 nm) have still significant smaller crystallite sizes than at 600 °C (Ce-11.7-600-I: 24.0 nm) treated samples. In a second cycle in soot combustion, the catalytic stability of the nanoscale ceria systems (Ce-16.4-400/600-I) was tested (Fig. 8). In the second run, the activity decreases to similar values of 514 °C (Ce-16.4-400-I) and 520 °C (Ce-16.4-600-I) compared to 414 and 461 °C in first combustion (Fig. 6). This deactivation is caused by the drastic increase of crystallite sizes after first catalytic combustion to 28.0 nm (Ce-16.4-600-I), 31.2 nm (Ce-16.4-600-I) in comparison to the original ranges of 9.6 and 14.nm, respectively. After the second cycle, almost no difference in size (38 nm) between different pre-annealed ceria particles is detected.

For industrial applications, particle growth and sintering effects of CeO_2 have to be minimized. Therefore the introduction of these catalytic active ceria nanoparticles inside temperature stable and chemical inert matrices like Al_2O_3, or SiC is necessary [33]. The latter is currently further developed using porous SiC matrices.

4. Conclusions

We have presented the preparation of nanosized cerium hydroxide and CeO_2 nanoparticles by inverse microemulsion technique using a non-ionic surfactant followed by thermal treatment at 100–600 °C. Due to the low viscosities of inverse microemulsions, our approach is suitable for the direct impregnation of porous SiC materials with well-defined ceria nanoparticles. A fundamental question is the size dependence of the catalytic activity, which can be addressed using inverse microemulsions due to the adjustable size of particles. The micelle and the particle size could be controlled in the narrow range of 5–16 nm varying the molar water to surfactant ratio from 5.8 to 16.4. The evaluation of micelle and particle sizes with comprehensive DLS and SAXS techniques for the first time confirms an increasing size with increasing R_W value. Crystallite sizes of ceria particles annealed at 100 and 400 °C with 6–16 nm show good agreement to sizes estimated for cerium hydroxide nanoparticles. For the first time, catalytic activity of microemulsion-derived ceria nanoparticles was studied in the soot combustion reaction, demonstrating higher catalytic activity of 400 °C treated samples ($T_{Max} = 404$ °C) compared to 600 °C ($T_{Max} = 461$ °C) caused by smaller crystallite sizes. During the first catalytic cycles, particle growth and sintering processes lead to crystallite sizes up to 31 nm after the TPO. This effect can explain the decreasing activity in the second cycle ($T_{Max} = 514$ °C). Our study shows the importance and need for encapsulation of catalytically active species for industrial applications.

5. Supporting information

S1 Pair distance distribution functions of inverse microemulsions and particle dispersions.

Appendix A. Supplementary materials

Supplementary data associated with this article can be found in the online version at doi:10.1016/j.jssc.2008.04.036.

References

[1] H.C. Yao, Y.F.Y. Yao, J. Catal. 86 (2) (1984) 254–265.
[2] E.E. Miro, F. Ravelli, M.A. Ulla, L.M. Cornaglia, C.A. Querini, Catal. Today 53 (4) (1999) 631–638.
[3] A. Trovarelli, Catal. Rev.-Sci. Eng. 38 (4) (1996) 439–520.
[4] T. Masui, K. Fujiwara, Y.M. Peng, T. Sakata, K. Machida, H. Mori, G. Adachi, J. Alloys Compd. 269 (1-2) (1998) 116–122.
[5] M. Fernandez-Garcia, A. Martinez-Arias, A. Iglesias-Juez, C. Belver, A.B. Hungria, J.C. Conesa, J. Soria, J. Catal. 194 (2) (2000) 385–392.
[6] E. Aneggi, C. de Leitenburg, G. Dolcetti, A. Trovarelli, Catal. Today 114 (1) (2006) 40–47.
[7] E. Aneggi, C. de Leitenburg, G. Dolcetti, A. Trovarelli, Top. Catal. 42–43 (1–4) (2007) 319–322.
[8] Q. Fu, A. Weber, M. Flytzani-Stephanopoulos, Catal. Lett. 77 (1–3) (2001) 87–95.
[9] Q. Fu, H. Saltsburg, M. Flytzani-Stephanopoulos, Science 301 (5635) (2003) 935–938.
[10] W. Bai, K.L. Choy, N.H.J. Stelzer, J. Schoonman, Solid State Ion. 116 (3-4) (1999) 225–228.
[11] L. Madler, W.J. Stark, S.E. Pratsinis, J. Mater. Res. 17 (6) (2002) 1356–1362.
[12] A.S. Deshpande, N. Pinna, P. Beato, M. Antonietti, M. Niederberger, Chem. Mater. 16 (13) (2004) 2599–2604.
[13] S.C. Laha, R. Ryoo, Chem. Commun. (17) (2003) 2138–2139.
[14] A. Corma, P. Atienzar, H. Garcia, J.Y. Chane-Ching, Nat. Mater. 3 (6) (2004) 394–397.
[15] T. Masui, K. Fujiwara, K. Machida, G. Adachi, T. Sakata, H. Mori, Chem. Mater. 9 (10) (1997) 2197–2204.
[16] A. Martinez-Arias, M. Fernandez-Garcia, V. Ballesteros, L.N. Salamanca, J.C. Conesa, C. Otero, J. Soria, Langmuir 15 (14) (1999) 4796–4802.
[17] J. Zhang, X. Ju, Z.Y. Wu, T. Liu, T.D. Hu, Y.N. Xie, Z.L. Zhang, Chem. Mater. 13 (11) (2001) 4192–4197.
[18] A. Bumajdad, M.I. Zaki, J. Eastoe, L. Pasupulety, Langmuir 20 (25) (2004) 11223–11233.
[19] V. Uskokovic, M. Drofenik, Surf. Rev. Lett. 12 (2) (2005) 239–277.
[20] H. Althues, S. Kaskel, Langmuir 18 (20) (2002) 7428–7435.
[21] O.P. Yadav, A. Palmqvist, N. Cruise, K. Holmberg, Colloid Surf. A 221 (1-3) (2003) 131–134.
[22] F.X. Chen, G.Q. Xu, T.S.A. Hor, Mater. Lett. 57 (21) (2003) 3282–3286.
[23] U. Natarajan, K. Handique, A. Mehra, J.R. Bellare, K.C. Khilar, Langmuir 12 (11) (1996) 2670–2678.
[24] E. Stathatos, P. Lianos, F. DelMonte, D. Levy, D. Tsiourvas, Langmuir 13 (16) (1997) 4295–4300.
[25] F.T. Quinlan, J. Kuther, W. Tremel, W. Knoll, S. Risbud, P. Stroeve, Langmuir 16 (8) (2000) 4049–4051.
[26] H. Herrig, R. Hempelmann, Nanostruct. Mater. 9 (1-8) (1997) 241–244.
[27] C. Beck, W. Hartl, R. Hempelmann, J. Mater. Res. 13 (11) (1998) 3174–3180.
[28] J. Henle, P. Simon, A. Frenzel, S. Scholz, S. Kaskel, Chem. Mater. 19 (3) (2007) 366–373.
[29] R. Palkovits, H. Althues, A. Rumplecker, B. Tesche, A. Dreier, U. Holle, G. Fink, C.H. Cheng, D.F. Shantz, S. Kaskel, Langmuir 21 (13) (2005) 6048–6053.
[30] H. Althues, P. Simon, S. Kaskel, J. Mater. Chem. 17 (8) (2007) 758–765.
[31] H. Althues, J. Henle, S. Kaskel, Chem. Soc. Rev. 36 (9) (2007) 1454–1465.
[32] H. Althues, R. Palkovits, A. Rumplecker, P. Simon, W. Sigle, M. Bredol, U. Kynast, S. Kaskel, Chem. Mater. 18 (4) (2006) 1068–1072.
[33] E. Kockrick, P. Krawiec, U. Petasch, H.-P. Martin, M. Herrmann, S. Kaskel, Chem. Mater. 20 (1) (2008) 77–83.
[34] B.J. Berne, R. Pecora, Dynamic Light Scattering, Dover Publications, Inc., New York, 2000.
[35] P. Scherrer, Nachr. Gött. (1918) 96–100.

[36] O. Glatter, O. Kratky, Small Angle X-ray Scattering, Academic Press, New York, 1982.
[37] D. Svergun, A. Semenyuk, 1992, GNOM 4.5.
[38] BrukerAXS, 2006, Nanofit 1.0.1.1.
[39] H.-D. Doerfler, Grenzflächen und kolloid-disperse Systeme, Springer, Berlin, 2002.
[40] A.N. Christensen, Acta Chem. Scand. 20 (3) (1966) 896–899.
[41] M. Wolcyrz, L. Kepinski, J. Solid State Chem. 99 (2) (1992) 409–413.